Modeling the spatial distribution of different strains of the COVID-19 virus based on the GeoSER(D) model

Yaroslav Vyklyuk *, Denys Nevinskyi, Valentyna Chopyak, Olga Golubovska, Kateryna Hazdiuk, Miroslav Škoda

Posted Date: 12 July 2023

doi: 10.20944/preprints202307.0775.v1

Keywords: multi-agent system; GEO-spatial simulation model; COVID-19; modelling; geo-object; real-time simulation.

Article

Modeling the Spatial Distribution of Different Strains of the COVID-19 Virus Based on the GeoSER(D) Model

Yaroslav Vyklyuk [1,*], Denys Nevinskyi [2], Valentyna Chopyak [3], Olga Golubovska [4], Kateryna Hazdiuk [5] and Miroslav Škoda [6]

[1] Department of Artificial Intelligence, Lviv Polytechnic National University, Lviv, Ukraine; vyklyuk@ukr.net
[2] Department of Electronics and Information Technology, Lviv Polytechnic National University, Lviv, Ukraine; nevinskiy90@gmail.com
[3] Department of Clinical Immunology and Allergology Danylo Halytsky Lviv National Medical University, Lviv, Ukraine; chopyakv@gmail.com
[4] Department of infectious diseases National medical university by A. A. Bogomolets, Kyiv, Ukraine; ogolubovska@gmail.com
[5] Department of Computer Systems Software, Yuriy Fedkovych Chernivtsi National University, Chernivtsi, Ukraine; kateryna.gazdyik@gmail.com
[6] Department of Management and Accounting, DTI University, 533/20, 018 41 Dubnica nad Va ̓hom, Slovakia; skoda@dti.sk
* Correspondence: vyklyuk@ukr.net; Tel.: +380950105036

Abstract: The paper proposed a modification of the GeoSER(D) model previously developed by us by detailing the age structure of the population, personal schedule on weekdays and working days, and individual health characteristics of the agents, this made it possible to build a more realistic model of the functioning of the city and its residents. The developed model made it possible to simulate the spread of 3 types of the strain of the COVID-19 virus, and to analyze the adequacy of this model in the case of unhindered spread of the virus among city residents. The paper showed that SARS COV 2 spreads mainly from contacts in workplaces and transport, and schoolchildren and preschool children are the consequence, not the initiator of the epidemic. Fluctuations in the dynamics of various indicators of the spread of SARS COV 2 associated with the difference in the daily schedule on weekdays and weekends. It has been shown that people's daily schedules strongly influence the spread of SARS COV 2. For the more contagious "rapid" strains of SARS COV 2 (omicron), immunocompetent people become a significant source of infection. For the less contagious "slow strains" (alpha) of SARS COV 2, the most active source of infection is immunocompromised individuals (pregnant women). The more contagious – "fast" strain of the SARS COV 2 virus (omicron) spreads faster in public transport. For less contagious – "slow" strains of the virus (alpha), the greatest infection occurs due to work and educational contacts.

Keywords: multi-agent system; GEO-spatial simulation model; COVID-19; modelling; geo-object; real-time simulation

1. Introduction

Viral infections have caused and continue to cause the largest epidemics humanity has ever encountered [1–3]. One of the greatest dangers they pose is their ability to mutate and give rise to new species and strains of viruses to which humans have no immunity. This includes SARS-CoV-2, coronaviruses, influenza viruses, and others. The problem of preventing the spread of viral infections is associated with several factors, including the presence of an incubation period and asymptomatic individuals. These factors make it impossible to detect such individuals without special diagnostics, and they, in turn, can infect others. Thus, there is a constantly active dynamic source of infection.

 doi:10.20944/preprints202307.0775.v1

Additionally, each viral infection has its own parameters of disease progression [4,5]. This, in turn, makes it impossible to establish universal rules for preventing an epidemic.

Vaccination is known to be one of the most effective methods of acquiring immunity and preventing the onset of an epidemic. However, it is only effective against known viruses, and in the case of new viruses, there is no vaccine available. Therefore, the most pressing task for humanity is to develop effective measures and policies that would prevent the onset of an epidemic and halt the spread of the virus at an early stage. Such measures should be implemented at various levels: cities, regions, countries, and globally. The most common preventive measures against epidemics include wearing masks, restricting people's mobility, implementing various degrees of quarantine, rapid and comprehensive diagnostics, and utilizing information technologies for contact tracing, among others. At the national and global levels, measures such as border closures, vaccination, and restrictions on travel between countries and regions are being implemented [6,7]. However, there are still no clear rules for preventing the spread of epidemics caused by new virus strains. The evidence for this is the rapid spread and global impact of the recent COVID-19 pandemic [1].

It is worth noting that current research focuses on various aspects of viral diseases. Some scientists concentrate on studying the viral infection itself [8]. Certain models simulate a virtual environment and the spread of viral infection within it, which is difficult to replicate in the real world [9]. Some researchers analyze the statistics and dynamics of infection spread and make predictions based on them for future trends [10–13]. However, this approach does not allow for predicting the dynamics of infection spread for new prevention strategies or new strains. This is because machine learning methods interpolate well within the training dataset, but they cannot forecast situations or analyze new factors that are absent from the training data.

Based on the above, it is currently relevant to develop a mathematical model and create a simulator program based on it for simulating the geo-spatial spread of viral infections at the city, regional, national, and global levels. Generally, the following requirements can be outlined for such a mathematical model:

1. It must be adequate and accurate.
2. It should be relatively straightforward.
3. It should be able to accommodate new factors.
4. It should consider the characteristics of viral infections.
5. It should realistically interpret human life and contacts:
    a. Taking into account the age and immune characteristics of individuals.
    b. Considering the specific daily routines of residents.
6. It should display results on a geographical map.
7. It should have fast calculations to enable a large number of computer experiments for training a neural network to determine the best epidemic prevention strategy.

The Materials and Methods should be described with sufficient details to allow others to replicate and build on the published results. Please note that the publication of your manuscript implicates that you must make all materials, data, computer code, and protocols associated with the publication available to readers. Please disclose at the submission stage any restrictions on the availability of materials or information. New methods and protocols should be described in detail while well-established methods can be briefly described and appropriately cited.

These requirements are met by the GeoCity model, developed by us in the work [42].

Therefore, the main objective of this study is to adapt, implement, and verify the adequacy of the multi-agent mathematical model GeoCity for modeling the geo-spatial spread of three different strains of the SARS-CoV-2 virus using the example of the city of Lviv, Ukraine, taking into account the peculiarities of the disease progression in different population groups.

 doi:10.20944/preprints202307.0775.v1

2. Literature Review

As mentioned above, there is no single approach to modeling the spread of new virus strains. There are numerous review papers that analyze and compare different approaches, their advantages, and disadvantages. In particular, the work [14] presents and discusses the main approaches used for monitoring and modeling the dynamics of infectious diseases. The fundamental concepts underlying their implementation and practice are explored, and an annotated list of representative works is provided for each category. The study [15] analyzes the methods of reporting systematic reviews and meta-analyses in evaluating healthcare interventions. The PRISMA methodology, consisting of a 27-item checklist and a four-phase flowchart, is discussed in detail.

As demonstrated in these works, the most appropriate methods for analyzing the spread of new virus species and strains, as well as evaluating new strategies and policies, are those based on multi-agent systems and cellular automata. They allow for simulating real human behavior and virus transmission in a virtual world, enabling virtual experiments. These models can be divided into two levels: pedestrian level and macro level (cities, states, and the world).

2.1. Pedestrian-Level Models

These models simulate human behavior in relatively small enclosed spaces and investigate virus transmission through human contact. For example, the study [16] presents a pedestrian-based epidemic spread model capable of simulating the risks of disease transmission in indoor environments during human social activities. In [17], the degree of contact between pedestrians at different pedestrian concentrations was determined through slow-motion recordings, serving as the basis for determining the probability of virus transmission. A microscopic pedestrian simulation model was considered in [18], where each agent represents an individual. Quantitative assessments of pedestrian infection risks were conducted in [19]. The infection of airplane passengers was studied in [20], while the clinical study of patient infection in a hospital was presented in [21]. These studies allow for establishing functional dependencies for the infection of individuals in confined spaces, providing a basis for constructing macro-level virus spread models.

2.2. Macro-Level Models

These models can be further divided into three groups: models based on static and movable cellular automata, as well as multi-agent systems.

2.2.1. Static Cellular Automata

Works that investigate mathematical models of static cellular automata include [22], where the developed model analyzed the impact of social isolation characteristics on population dynamics, simulated the number of COVID-19 deaths due to the absence of healthcare infrastructure, and studied the effect of healthcare system actions on the crisis in Brazil. Effective modeling of the dynamics of infectious disease spread in spatially constrained environments is presented in [23], which examines the interaction between humans and pathogens using the example of tuberculosis transmission. In [24], a SLIRDS model (Susceptible-Latent-Infected-Recovered-Dead-Susceptible) was created based on cellular automata theory and compartmental models, which can better reflect the actual infectious process of infectious diseases. Using the SLIRDS model, the complex process of pandemic influenza A (H1N1) spread was simulated. The use of cellular automata (CA) for creating an epidemic computational model of virus spread in supermarkets under various conditions is analyzed in [25], employing an approach that has not been used before. In [26], a 2D cellular automaton based on the SI epidemic model is proposed to determine the most desirable testing frequency and the optimal size of random traces in local urban environments for diagnosing SARS-CoV-2 and isolating infected individuals.

 doi:10.20944/preprints202307.0775.v1

2.2.2. Movable Cellular Automata

The application of movable cellular automata for predicting the spread of the SARS-CoV-2 virus in countries such as Turkey, Ukraine, Serbia, and Slovakia was conducted in a study [27]. The study proposed a model that allowed for the comparison of simulation models with real regions and countries in terms of time and scale. The accuracy of this model was demonstrated, and an analysis of different strategies for preventing viral infection spread was performed. In another study [28], spatial factors influencing physical distancing and their impact on the transmission of the SARS-CoV-2 virus were investigated by integrating pedestrian dynamics with a modified susceptible-infectious-recovered model. The generalization of a mathematical model for determining the temporal evolution of the population in infectious diseases of the COVID-19 pandemic, based on the Kermack-McKendrick model, was explored in a study [29]. An article [30] proposes a new optimization algorithm for COVID-19 (CVA) that covers almost all possible optimization problem domains. It also models the process of coronavirus spread in multiple countries worldwide and the spread of the coronavirus as an optimization problem to minimize the number of countries infected with SARS-CoV-2. Three scenarios for solving the optimization problem using the most effective distribution factors were proposed. In a study [31], a stochastic structure based on movable agents was developed, allowing for the modeling of clinical and social heterogeneity. All these models are more adequate for real social systems, although they are significantly slower.

2.2.3. Multi-Agent Systems

In contrast to movable cellular automata, which resemble the movement of molecules in a closed environment, multi-agent systems operating according to a daily schedule provide a more realistic simulation of the functioning of a city, region, or country as a whole. Moreover, they are considerably faster than movable cellular automata. This approach was demonstrated in a study [32], which described the development and implementation of an agent-based epidemiological modeling system. A similar model allows for the modeling of the dynamics of SARS-CoV-2 spread among city residents and is described in a study [33]. In the research [34], the modeling results of COVID-19 spread in a limited region with specific demographic characteristics and social relations were presented. This study aims to explore the impact of preventive methods, such as quarantine, social distancing, and reduction of mass transportation, on the spread of epidemics. The adequacy and speed of these models enable their use for automatically determining optimal pandemic prevention strategies and optimal government policies, as presented in the study [35]. This article investigates how reinforcement learning (RL) can be used to optimize a mitigation policy that minimizes the economic impact without overwhelming hospital capacity. In the research [36], multi-agent modeling (MAS) is used to examine the optimal strategy for preventing the spread of COVID-19 in Japan. Different recommendations for optimal strategies to suppress the pandemic by combining reinforcement learning and MAS were also proposed. This study highlights the potential of MAS in developing infection prevention strategies.

2.2.4. Geospatial Models

Despite the power and capabilities of these models, one drawback is the lack of visualizing results on a geographic map. Such a representation of results would allow for a visual assessment of the scale and dynamics of infection spread. There is a series of works that utilize cellular automata for these purposes, including the study [37], which presents the Flu And Coronavirus Simulator (FACS), a modeling tool that simulates virus spread at a subnational level, including geospatial data sources to identify buildings and residential areas within a region. FACS enables modeling the spread of COVID-19 at the local level and provides estimates of infection spread and hospital admissions for different scenarios. The geospatial spread of SARS-CoV-2 on Chikungunya Island was investigated in a study [38].

Preprints (www.preprints.org) | NOT PEER-REVIEWED | Posted: 12 July 2023 doi:10.20944/preprints202307.0775.v1

3. Materials and Methods

To eliminate ambiguities in the terminology of multi-agent systems (MAS) theory and medicine, we introduce the following definitions:

- respondent in medicine is defined as an agent in MAS;
- viral infection in medicine refers to a set of rules and properties in MAS.

In this work, we have expanded the functionality of the GeoCity model (1) proposed by us in [42]. The model is based on a dynamic multi-agent system that incorporates individual health characteristics of agents (H) and rules for the spread of the SARS-CoV-2 virus (V).

$$\text{GeoCity}=\{G,T,A,R,H,V\}_{\text{city}} \quad (1)$$

Here, G represents a set of geo-objects, T denotes transport, A is the list of agents residing in the city, R represents daily schedule rules for agents, and there is a set of data describing interaction processes. This includes the health status of an agent (H) and the rules for the spread of infection upon contact with infected and healthy agents (V).

Similar to the work in [42], we considered the following locations that agents (humans) visit: childcare centers, schools, universities, offices, supermarkets, and shops. Accordingly, we took into account the age of people, which determines the locations they visit. The age of respondents also affects their medical indicators, such as contagious level and immune system condition. We also considered a 24-hour day and time discretization of the model with an interval of 1 hour. For each individual, a unique hourly schedule was constructed for both weekdays and weekends.

The model itself consists of three stages. The first stage involves initializing the virtual city and its population, as described in [42]. The second stage consists of the initialization of parameters related to the viral infection. The final stage is the simulation of the city's functioning and the spread of the viral infection, considering hourly time intervals and accounting for working days and weekends.

3.1. Stage 1: Model Initialization

The model was initialized following a similar approach as in the work [42]. The main differences were related to agent generation. Specifically, we took into account the following age groups: Children (0-6), Pupil (7-17), Young (17-44), Adult (45-60), Aged (60-). The age of each person (age) within a group was randomly generated within the corresponding age range. Depending on their age, individuals could have different professions. For example, children aged 0 to 4 could either stay at home or attend a childcare center. An adult living with a minor child was assigned the profession of "mother." Children aged 4 to 14 were considered pupils. People aged 15 to 24 could be university students or employed. Individuals over the age of 65 were considered retirees. All other individuals between the ages of 25 and 64, as well as young adults of student age who were not students, could work in professions such as office worker, store clerk, salesperson, or public transportation driver. Agents without a profession were marked as unemployed.

To simulate the spread of the virus, it was necessary to indicate the immune system state h_i of each individual a_i during the model initialization stage. This state was described using the following parameters:

- Health status (S_i = ["S","E","I","R"("D")]): S – susceptible, E – exposed, I – infected, R – recovered, or D – deceased (at the initial stage, all individuals were healthy (S)).
- Immunity status ($im_i = [0,1]$): 0 represents no immunity to the infection, and 1 represents 100% immunity (recovered individuals).
- Contagiousness level ($con_i = [0,10]$): determines the infectiousness of a specific infected person, indicating how likely they are to infect others.
- Asymptomatic status ($sym_i = True/False$): indicates whether a person will exhibit symptoms or be asymptomatic when infected.

Preprints (www.preprints.org) | NOT PEER-REVIEWED | Posted: 12 July 2023 doi:10.20944/preprints202307.0775.v1

- Contagiousness level on a specific day t – con_i^t.
- Infection time, t_i^{inf} (days).
- The number of people infected by the agent, R_i.

$$H = \{h_i\}_{i=1,P} = \{\boldsymbol{a_i}, \boldsymbol{S_i}, \boldsymbol{im_i}\ \boldsymbol{con_i}, \boldsymbol{sym_i}, con_i^t, t_i^{inf}, R_i\}_{i=1,P} \quad (2)$$

Here, a_i represents the agent identifier, P denotes the number of agents.

These characteristics depend on individual parameters, such as age and pregnancy status in women. Pregnancy status is randomly determined for adult individuals based on statistical data [43].

3.2. Stage 2: Initialization of Rules for the Course of Viral Infection V

By these rules, we understand how agents' health parameters h_i will change during interaction with other agents and throughout the disease. Unlike other model attributes, these rules are described using functional dependencies under the SEIR(D) approach.

$$V = \{con(t_{st}), St_{inf}(P_{inf}), St_{R(D)}(t_{st}, \quad t_i)\}, \quad (3)$$

here $con(t_{st})$ is the function that determines the contagiousness level of the infected agent, $St_{inf}(P_{inf})$ the function that determines the change of state for a susceptible agent after contact with an infected agent, P_{inf} the function representing the probabilities of infection, and $St_{R(D)}(t_{st}, t_i)$ is the function that determines whether an infected agent will recover or die after experiencing the illness. Let's consider each of these functions in turn.

3.2.1. Contagiousness

According to the classical SEIR(D) model, agents can be in four stages: "S" – susceptible, "E" – exposed, "I" – infected, and "R" ("D") – recovered or deceased. The lifecycle of a real agent consists of the following steps. A susceptible person can interact with an infected agent, and with some probability, the susceptible agent can be infected. Upon infection, the agent transitions to the "E" state, where it doesn't exhibit symptoms but can infect others. After a certain time, t_i, the agent transitions to the "I" state, indicating the presence of symptoms. Eventually, after time t_r, the agent either recovers ("R") or dies ("D"). Studies [36] have shown that for real illnesses, another dependency of infectivity or contagiousness is observed. After infection, an agent is initially asymptomatic and cannot infect other people. After some time, $t_c < t_i$, the agent becomes capable of infecting others with varying probabilities. After time t_i, the agent develops symptoms of the illness. These times vary for different types of illnesses. During the lifecycle, the contagiousness of the agent changes, reaching maximum values at the end of the "E" state and the beginning of the "I" state. We propose describing the level of contagiousness using the L-R membership function from fuzzy logic, which is used to describe natural processes.

$$con(t_{st}) = \begin{cases} t_{st} \le t_i & \max\left(0, Real\left(\sqrt[2]{1 - \left(\frac{t_i - t_{ts}}{a}\right)^2}\right)\right), \\ t_{st} \ge t_i & e^{-\left|\frac{d - t_i}{b}\right|^3} \end{cases} \quad (4)$$

here, t_{st} is the time during which the agent is in the same state, and a and b are empirical parameters.

For COVID-19, the duration of the "E" state without contagiousness strongly depends on the virus strain. Additionally, it can vary significantly within a particular strain based on individual characteristics and the date. For example, for the alpha strain, it can range from 4.5 to 22 days. To ensure the adequacy of the model, we will assume 12 days for this period [41]. After this period, the

Preprints (www.preprints.org) | NOT PEER-REVIEWED | Posted: 12 July 2023 doi:10.20944/preprints202307.0775.v1

agent can infect others for 2 days, leading to t_i = 14 days. The symptomatic phase begins after this period and can be described by equation (12) with $a = 5$ and $b = 9$ (see Figure 1).

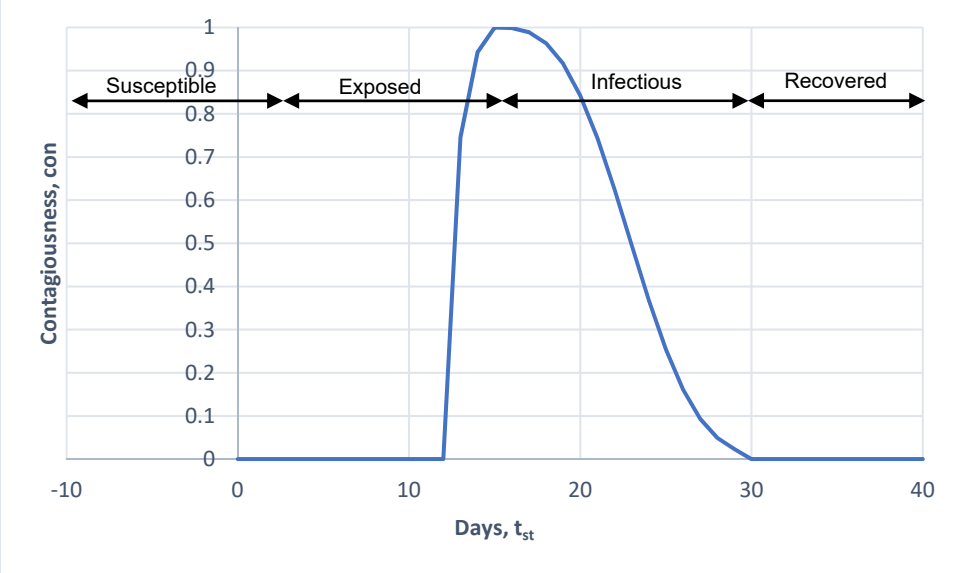

Figure 1. Contagiousness of infected agent dependency on time.

In this approach, we can merge "E" and "I" state. It means that the agent is infected with different levels of contagiousness.

3.2.2. Infecting:

As previously mentioned, agents interact in various locations such as workplaces, supermarkets, and transportation, as well as within their families throughout the day. We will explore two approaches to model the connection between agents: the multi-agent approach [36] and probability theory. Considering the distinct behavior of agents in these locations, using either approach will result in an increase in the number of iterations and time required. In a study [42], the following approach was proposed: if a susceptible person is present in a location where infectious individuals also reside on the same day, the probability of infection can be calculated as follows:

$$P_{inf} = \left(\frac{LS_s}{OD_{loc}} \times \frac{LS_i}{A_{con}}\right) \times \frac{IR}{360} \times M \quad (5)$$

here, P_{inf} presents the probability of a susceptible person becoming infected. LS_s is the duration of stay of the susceptible person in minutes, LS_i is the duration of stay of the infectious person in minutes, OD_{loc} is the opening duration of the location on that particular day, A_{con} is the area of the location in square meters, IR is the infection rate (e.g., 0.07), and M is a static contact rate multiplier with a default value of 1.

It should be noted that in our approach, LS_s, LS_i, and OD_{loc} are approximately equal for each area. Obtaining precise information about the area of each location in a real city is challenging. Instead of the room area, we suggest using the number of contacts in the room. If, on average, one agent can come into contact with n agents in a specific location during one iteration, then the probability of infection will be inversely proportional to the total number if there are more than n people in the workplace, transportation, or supermarket. This is because an infected person cannot contact all of them. Conversely, if there are only two people in the room, the contact time and the probability of infection will increase accordingly. Therefore, we propose modifying formula (5) as follows:

$$P_{inf} = LS_i \times \frac{IR}{360} \times N_{inf} \times \frac{n}{N_{obj}} \times \sum_{a=1}^{N_{inf}} con_a \times (1 - imm). \quad (6)$$

Preprints (www.preprints.org) | NOT PEER-REVIEWED | Posted: 12 July 2023 doi:10.20944/preprints202307.0775.v1

Here, N_{obj} represents the number of agents in a specific location, con_a is the level of contagiousness of agent a, and imm is the level of immunity of a susceptible agent. If there are N_{inf} infected agents in the same location, the probability should be proportionally increased.

Based on the obtained probability of infection, a change in the state of a susceptible agent is determined as:

$$\boldsymbol{St_{inf}\left(P_{inf}\right)=\begin{cases} I & x < P_{inf} \\ S & x \geq P_{inf} \end{cases}} \quad (7)$$

here, x ∈ [0,1] represents a random number.

3.2.3. Recovering

An infected agent can either recover or die, depending on its probability of death. Recovery occurs when an infected agent becomes ill and its infection level falls below a certain small threshold:

$$\boldsymbol{St_{R(D)}(t_{st}, \quad t_i)=\begin{pmatrix} R & x \geq P_{death} \\ D & x < P_{death} \end{pmatrix}_{t_{st}>t_i \text{ and } con(t_{st})<\alpha}} \quad (8)$$

Here, α represents the threshold level of contagiousness.

3.3. Stage 3: Simulating the Functioning of the City and Virus Spread

This stage consists of the following steps.

3.3.1. Step 1: Initial Infection

Before starting the simulation, it is necessary to define the source of infection. It should be noted that the model is probabilistic and heavily dependent on the initially infected individual, including their interactions, cohabitation, and daily schedule. Therefore, during the initial stages of modeling, significant fluctuations in all statistical parameters are possible. To reduce the impact of stochasticity and facilitate convergence to the laws of large numbers, several infected individuals should be used as the source of infection. In our calculations, we considered a group of 10 infected individuals.

3.3.2. Step 2: Determining the Health Status of Individuals at the Beginning of the Day

At the start of the working day, the infection duration for each infected individual is increased by 1 day. Their personal level of contagiousness at the beginning of the day is also recalculated based on the number of days they have been sick (t_j) according to equation (2) and their personal level of contagion:

$$con_i^t = con(t_i) \times con_i \quad (9)$$

For non-infected individuals, $con_j^t = 0$.

3.3.3. Step 3: Simulation of the Working Day

During this stage, based on the schedule (considering working days and weekends), the location of each individual is determined hourly. The objects $(v \subset J)$ where infected individuals are present are identified for each hour. The number of infected individuals present in each object (N_{inf}^v) is determined. For each healthy individual located near infected individuals, the probability of infection is calculated using formula (6). The status of healthy individuals (S) is then changed to infected (I) according to equation (7).

In case of a change in the health status of a healthy individual, the coefficient R_j is increased symmetrically for each infected individual to the level of con_j^t.

Preprints (www.preprints.org) | NOT PEER-REVIEWED | Posted: 12 July 2023 doi:10.20944/preprints202307.0775.v1

3.3.4. Step 4: End of the Working Day

At the end of the simulation of the working day, the possibility of recovery or death is determined for all infected individuals according to formula (8). Statistical data is analyzed and saved, including the calculation of the reproductive number, that define as an average number of infected people by sick agent:

$$R_0 = \overline{(R_j)}_{R_j>0}$$

The simulation continues until there are no infected individuals left or until it is forcibly stopped.

4. Results and Discussion

4.1. Population Generation

The purpose of this work was to test the relevance (adequacy) of the proposed model for simulating three variants of SARS-CoV-2, namely Alpha, Delta, and Omicron. In this analysis, we will not consider any means of preventing the spread of these viral infections by the government. In other words, we will try to simulate the spread of infections without any human or governmental response, which will allow us to observe how the infection would develop on its own and what consequences it would lead to.

Each of these variants of coronavirus strains possesses distinct characteristics. There are eight major variants of the novel coronavirus SARS-CoV-2 that are of concern to medical professionals at the moment. In the summer of 2021, the World Health Organization decided to designate SARS-CoV-2 variants using letters from the Greek alphabet instead of using the names of countries where they were detected. It all started with the variant L, which was detected in Wuhan, China, in December 2019. The most prevalent variants on the European continent, including Ukraine, are Alpha, Delta, and Omicron. It is these particular variants that we have taken into account in this study.

The "Alpha" variant - B.1.1.7 (Kent or British variant) has specific symptoms: cough, severe fatigue, sore throat, and muscle pain, with loss of smell and taste occurring rarely. The "Alpha" variant spreads more quickly compared to the original Chinese variant.

The "Delta" variant - B.1.617.2 (Indian variant) causes leading symptoms such as headache, sore throat, malaise, and fever. Patients infected with the Delta variant mention cough and loss of smell much less frequently. According to Indian doctors, people infected with the Delta variant more often experience hearing loss, severe abdominal pain, and nausea. They also complained of dryness in the mouth, loss of appetite, and joint pain. In most cases, these patients were hospitalized more frequently, requiring oxygen therapy and suffering from the development of complications.

The "Omicron" variant - B.1.1.529 (South African variant) is highly transmissible. It generally has a milder course compared to the Delta variant, with symptoms such as sore throat, malaise, and slight temperature elevation. Patients with the Omicron variant require professional medical assistance much less frequently.

"Omicron" is capable of increasing reinfection rates by eight times. It reduces the effectiveness of the Pfizer vaccine in preventing hospitalization after two doses to 70%.

Mathematically, the level of contagion depending on the duration of infection can be described using the following graphs (Figure 2).

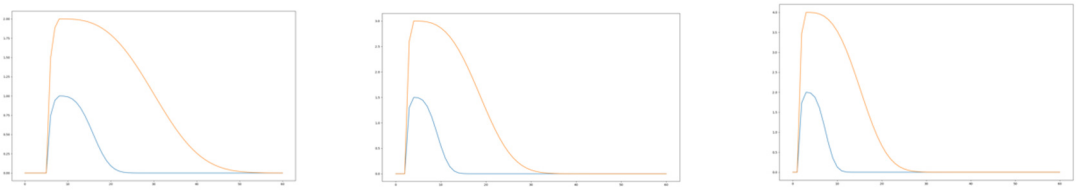

(Alpha) (Delta) (Omicron)

Figure 2. Contagiousness (12) of infected agent dependency on time for different stamp of viruses: Alpha $t_i = 15, a = 3, b = 9$, Delta $t_i = 4, a = 2, b = 6$, Omikron $t_i = 3, a = 2, b = 5$

 doi:10.20944/preprints202307.0775.v1

So, as can be seen from the contagion graphs, the Omicron and Delta variants have the shortest incubation period and are characterized by a rapid course of the disease. In contrast, the Alpha strain has a long incubation period and a prolonged period of illness, during which infected individuals can transmit the infection to others. The graphs clearly show that considering contagion leads to both a higher level of infectiousness in individuals and a longer period of potential transmission to others.

It is believed that the immune system status of respondents affects contagiosity. According to statistical data [45,49], all respondents are divided into immunocompetent (55%) and immunocompromised (45%) individuals. The group of physiologically immunocompetent individuals includes 50% of people aged 18 to 65 years who harmoniously respond to contact with infectious agents and recover quickly. This is the majority of the population.

This group also includes 5% of people who have a very well-developed genetically based anti-infectious immunity. They can carry various strains of coronavirus asymptomatically, as well as other infections.

The group of immunocompromised individuals includes physiological and pathological subgroups. Physiological immunocompromised subgroups include children (10%) and the elderly 65+ (10%), who are more susceptible to infectious diseases due to age-related peculiarities of immune response to infections. In addition, the incubation period is 2-3 days longer in children and 1-2 days longer in the elderly compared to immunocompetent individuals. Pregnant women (5%) are also included in this physiological subgroup of immunocompromised individuals.

Pathologically immunocompromised individuals include those with genetic immunodeficiencies and people with immune disorders. Up to 1% of people may have significant genetic defects in the immune system and therefore cannot fight off many infections, including coronavirus infection. It has been established that up to 19% of respondents have acquired immune system disorders as a result of immune system dysfunction, leading to chronic diseases (diabetes, hypertension, kidney diseases, etc.), long-term use of immunosuppressive drugs (oncological, autoimmune diseases, post-transplantation), or an unhealthy lifestyle (smoking, obesity, etc.).

4.2. City Simulation

The spread of these coronavirus variants was examined through a simulation of Lviv, Ukraine. Lviv is the largest regional center in western Ukraine, with a population of about 700,000. The city has a circular shape for its center, while the city borders have a complex structure with multiple branches (Figure 3).

The simulation was conducted with the following parameters: 10,000 agents, 3,000 homes, 100 grocery stores, 3 preschools, 7 schools, 2 universities, 50 retail stores, 100 transportation hubs, and 50 office buildings. According to statistics [43], only 20% of Ukrainians own a car, which means that 80% of the population use public transport or walk. In our simulation, 50% of the agents use public transport, while 30% are pedestrians.

According to statistical data [43], 60% of children attend preschool, and students make up 80% of the student-age category. Additionally, 6% of people are unemployed. We assume that one family member visits a supermarket near their place of residence after work. Individuals who do not work (mothers, unemployed) and stay at home during the day, on average, visit 2-3 supermarkets and 1 clothing store.

Preprints (www.preprints.org) | NOT PEER-REVIEWED | Posted: 12 July 2023 doi:10.20944/preprints202307.0775.v1

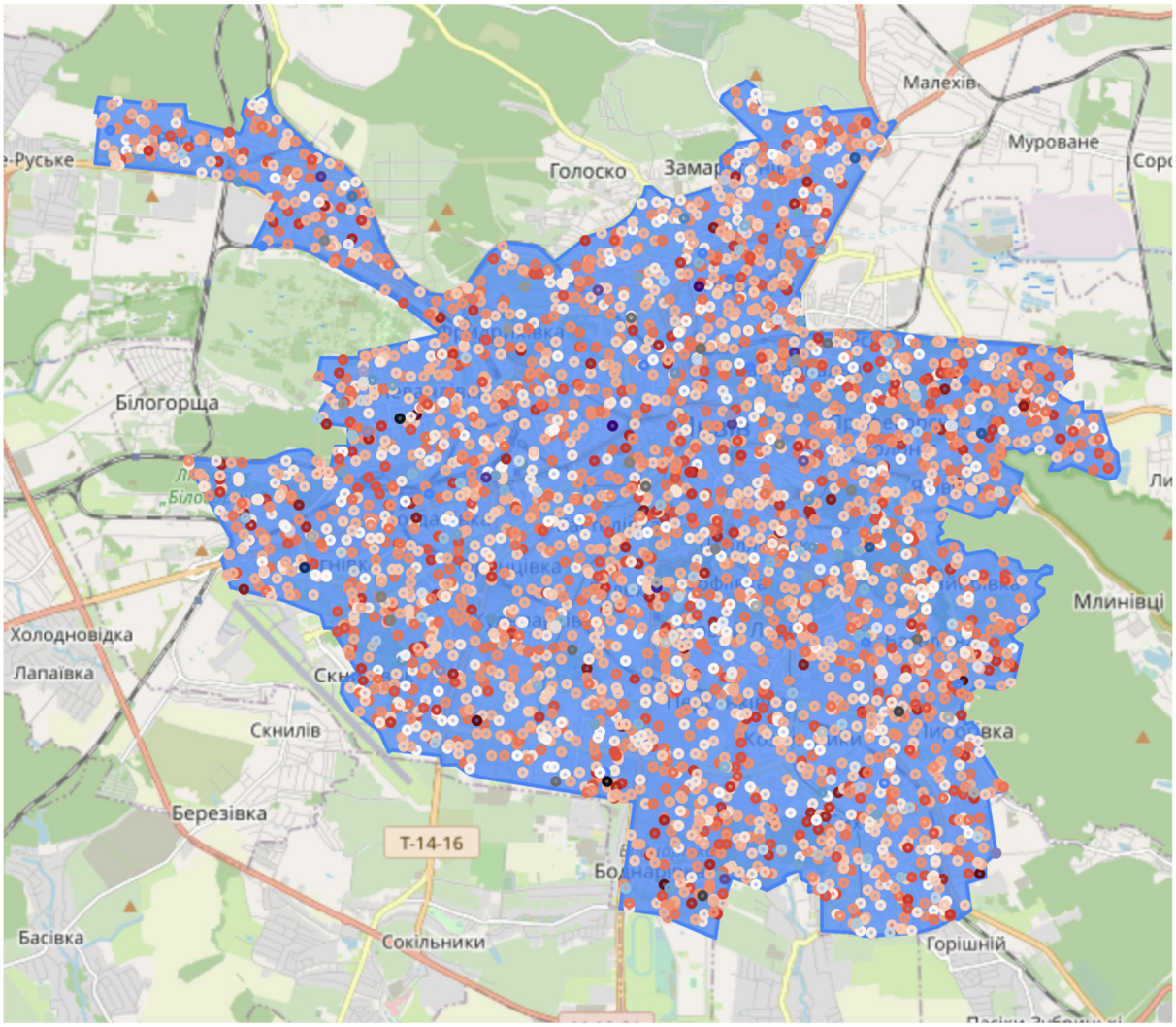

Figure 3. Simulated city Lviv, Ukraine

The statistics of job positions obtained after the city simulation are presented in Table 1.

Table 1. Number of people working in different job positions.

Object	Workers
Grocery	1000
Offices	3240
Preschools	570
Schools	1330
Retail	500
Transport	100

As mentioned above, each individual is assigned a job position. The distribution of job positions and age groups obtained is presented in Table 2.

Preprints (www.preprints.org) | NOT PEER-REVIEWED | Posted: 12 July 2023 doi:10.20944/preprints202307.0775.v1

Table 2. Distribution of people by age and professions.

Age Group	Job	Number
Adult	Offices	3141
Aged	Domestic	1739
Pupil	School_pupil	1109
Adult	Grocery	960
Student	University_Student	757
Adult	Retail	487
Adult	Unemployed	328
Adult	Domestic	321
Adult	Schools	271
Children	Preschool_Chield	244
Children	Domestic	169
Adult	PreSchools	116
Adult	Transport	98
Student	Offices	99
Adult	Universities	76
Student	Grocery	40
Student	Retail	13
Student	Unemployed	11
Student	Schools	9
Student	Universities	4
Student	PreSchools	4
Student	Transport	2

As seen from the table, the largest number consists of office workers. Young individuals of student age are not only students but also work in various professions. It can also be observed that the number of individuals taking care of children and unemployed middle-aged people is approximately the same.

4.3. Modeling the Spatial Spread of the Alpha Variant Virus

Figure 4 presents the simulated weekly dynamics of the spread of the coronavirus infection throughout the entire epidemic process. Infected individuals' houses are marked with red dots, uninfected ones with green, and gray dots represent those who have recovered.

As seen from the figures, there is no observed epidemic in the first month. The following two months witness a sharp increase in the number of infected individuals. Then, a rapid decline in the epidemic is observed. Additionally, from the figures, it is evident that a large number of residential buildings remained uninfected. The total duration of the epidemic lasted for four months. Moreover, it can be observed that the infection spreads evenly across the entire city, with no distinct clusters of infection.

A more visual representation of the infection dynamics is presented in Figure 5. As seen from the figure, the peak of the epidemic occurred on the 40th-50th day (considering a 5-day incubation period, it corresponds to the 35th-45th day from the onset of the first symptoms). Additionally, the graph shows slight fluctuations in the dynamics trend, which can be attributed to different daily schedules of people during weekdays and weekends. The figure also indicates that approximately 20% of people remained uninfected. The dynamics of the reproduction number (Figure 6) is interesting. It can be observed that this indicator fluctuates significantly during the initial stage of the epidemic, reaching a value of 6. Gradually, by the 40th day, it stabilizes at around 3.8, which aligns well with experimental data [43].

Preprints (www.preprints.org) | NOT PEER-REVIEWED | Posted: 12 July 2023 doi:10.20944/preprints202307.0775.v1

Figure 4. Simulated weekly dynamics of the Alpha variant spread in Lviv city.

Preprints (www.preprints.org) | NOT PEER-REVIEWED | Posted: 12 July 2023 doi:10.20944/preprints202307.0775.v1

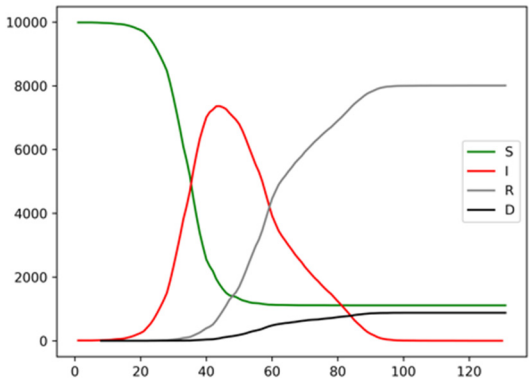

Figure 5. Dynamics of the number of infected, healthy, recovered, and deceased individuals in the simulation of the Alpha variant.

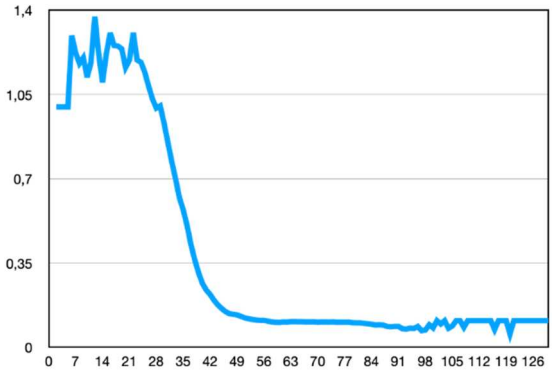

Figure 6. Dynamics of the reproductive number R_0 in the simulation of the Alpha variant.

The dynamics of immunocompromised and immunocompetent individuals are also intriguing. Despite the lower overall immunity of immunocompromised individuals to various infections, their relative number affected by the coronavirus infection is only slightly higher than that of immunocompetent individuals (Figure 7), considering that almost all healthy individuals also get infected. Furthermore, from the graphs, it can be observed that immunocompromised individuals become infected faster than immunocompetent ones, reaching a rate of 86% on the 43rd day from the start of infection. This is particularly evident from Table 3, where 25% of infection among immunocompromised individuals is reached on the 28th day, whereas the same level for immunocompetent individuals is achieved in 32 days, i.e., 4 days later. The 50% infection level among immunocompromised individuals occurs 5 days earlier than in immunocompetent individuals. Thus, the peak of the epidemic for immunocompetent individuals occurs approximately one week later than for immunocompromised individuals. The maximum infection rate for immunocompetent individuals is 75%. Additionally, from the graph, it can be seen that immunocompromised individuals have a significantly longer duration of illness. Moreover, their dynamics show a slight peak on the 65th day, which is due to children having a longer incubation period, thus experiencing the peak of the disease later, as will be shown further.

Preprints (www.preprints.org) | NOT PEER-REVIEWED | Posted: 12 July 2023 doi:10.20944/preprints202307.0775.v1

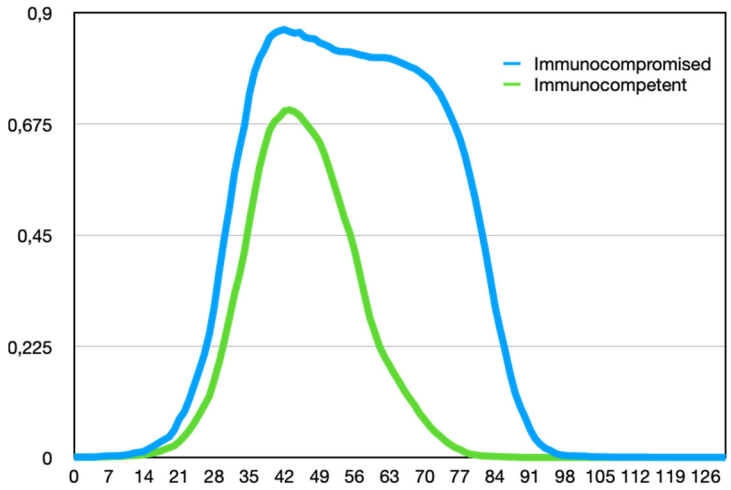

Figure 7. Comparative dynamics of the number of immunocompromised and immunocompetent individuals in the simulation of the Alpha variant.

Table 3. Number of days to reach the specified infection level for the Alpha variant depends on immunity.

	Immunocompromised	Immunocompetent	Difference
25%	28	32	4
50%	32	37	5
75%	37	44	7
86%	43		

As immunocompromised individuals become infected earlier and have a higher level of contagion, they can indeed infect significantly more healthy people (Figure 8). Therefore, their reproductive number (R_0) is significantly higher (R_0 =5.8) compared to immunocompetent individuals (R_0=1.7). Consequently, immunocompromised individuals are much more dangerous for the spread of the epidemic.

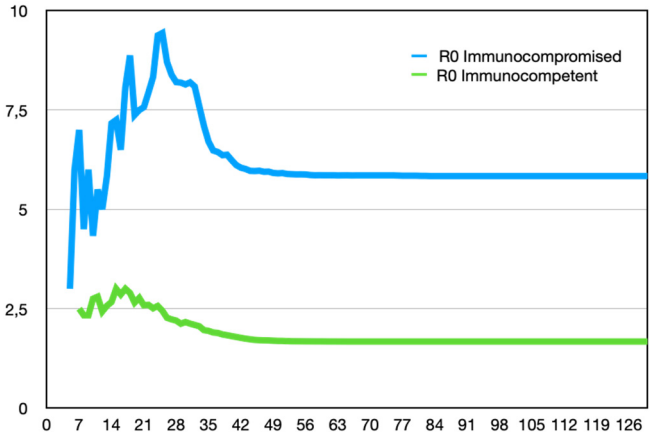

Figure 8. Comparative dynamics of the reproductive number (R_0) for immunocompromised and immunocompetent individuals in the simulation of the Alpha variant.

Of particular interest is the comparison of infection spread among people in different age groups, taking into account the group of pregnant women. The results are presented in Figure 9. As can be seen from the graph, a distinct group of young people aged 0 to 18 years stands out. As

Preprints (www.preprints.org) | NOT PEER-REVIEWED | Posted: 12 July 2023 doi:10.20944/preprints202307.0775.v1

mentioned earlier, they have an incubation period that is 3 days longer. This means that in the case of an active virus, schoolchildren and children attending daycare are more likely to be infected by individuals from other groups in their place of residence rather than within their own group (school, daycare). These children form somewhat closed systems, which results in a significantly lower number of infected children compared to other groups, despite their higher level of contagion.

As mentioned earlier, older individuals have a 2-day longer incubation period. However, this period is not sufficient to exhibit behavior similar to that of young people.

Interesting results were obtained when analyzing the reproductive number (Figure 10). As seen from the figure, pregnant women infect the highest number of people. This is due to their high level of contagion and having a similar work week as ordinary people. Despite the higher level of contagion in the elderly, they exhibit lower values of the reproductive number. This is due to their limited social interactions during the epidemic. People with normal immune function infect a significantly larger number of healthy individuals due to their active lifestyle. This is observed for young and middle-aged individuals without restrictions. It should also be noted that preschoolers and schoolchildren infect fewer other people due to their longer incubation period. By the time they can infect others, the people around them are already either sick or immune. Therefore, this group of people is a consequence, rather than an initiator, of the epidemic.

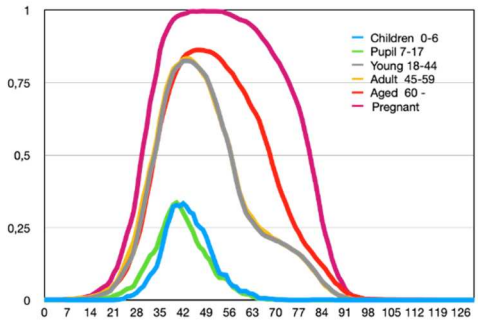

Figure 9. Comparative dynamics of the number of infected individuals in different age groups in the simulation of the Alpha variant.

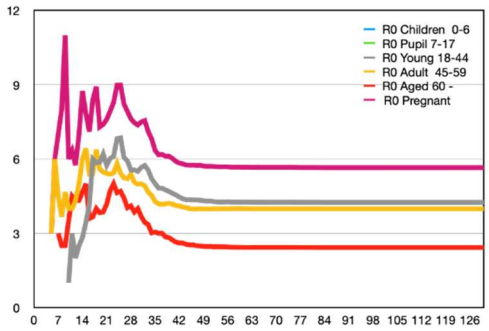

Fig. 10. Comparative dynamics of the reproductive number in different age groups in the simulation of the Alpha variant.

Different behaviors are observed among people depending on their mode of transportation: public transport or private cars (walking). The infection dynamics for these individuals are nearly identical. This is because the highest number of contacts occurs on workdays. However, people using public transport infect a larger number of other people (R_0=3.9 for public transport, R_0=3.4 for private cars), as reflected in the reproductive number (Figures 11 and 12). It should be noted that people using public transport become infected on average 3-5 days earlier than those using private cars or walking (Table 4). There is also a significant difference in the maximum number of people infected. In public transport, 81% of people get infected, while those using private cars (or walking) account for 60%, which is 21% less.

Preprints (www.preprints.org) | NOT PEER-REVIEWED | Posted: 12 July 2023 doi:10.20944/preprints202307.0775.v1

Table 4. Number of days to reach the specified infection level for the Alpha variant depends on type of transport.

	Public Transport	Private Cars (Walking)	Difference
25%	30	33	3
50%	34	39	5
75%	40		

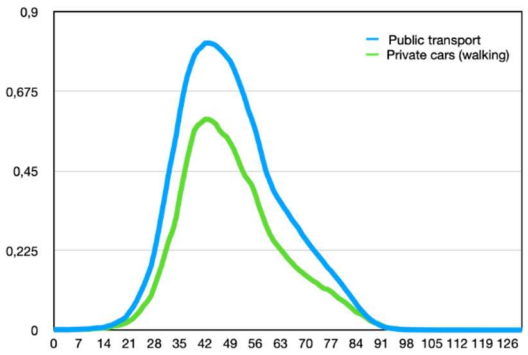

Figure 11. Comparative dynamics of the number of infected individuals depending on transportation in modeling the Alpha strain.

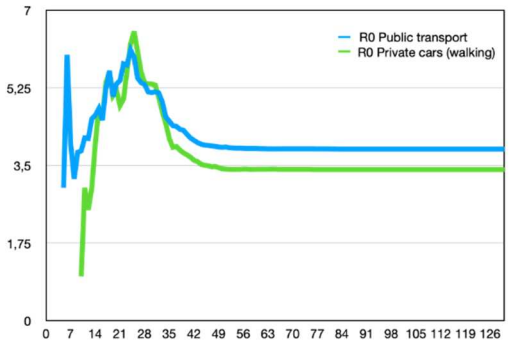

Figure 12. Comparative dynamics of the reproductive number depending on transportation in modeling the Alpha strain.

A similar analysis regarding professions (Table 5) shows that the highest level of infection is observed in professions such as universities and offices. These institutions have the highest number of contacts between infected and healthy individuals, thus resulting in the highest level of transmission.

Table 5. Reproductive number for different professions for the Alpha strain.

Proffesion	R_0
University_Student	6,4
Offices	4,4
Universities	4,1
Grocery	3,6
Schools	3,5
Retail	3,2
PreSchools	3,1
Unemployed	2,3

Preprints (www.preprints.org) | NOT PEER-REVIEWED | Posted: 12 July 2023 doi:10.20944/preprints202307.0775.v1

Domestic	2,0
Transport	2,0

4.4. Modeling the Spatial Spread of the Delta Variant

According to the geospatial modeling of the spread of this coronavirus strain, it spreads uniformly throughout the city, similar to the previous case, but at a much faster rate. This can be observed from the graph depicting the dynamics of the number of infected individuals (Figure 13). As seen, the peak of the epidemic occurs on the 18th to 20th day after the onset of infection. The number of uninfected individuals remains approximately at the same level. Weekly fluctuations in the dynamics of infection spread to become more pronounced.

The reproductive number is slightly higher, reaching 6.0 (Figure 14). Within a shorter period of time, infected individuals have the opportunity to come into contact with slightly fewer people in their surroundings. Therefore, the increase in the reproductive number is specifically associated with the increased contagiousness of the virus itself.

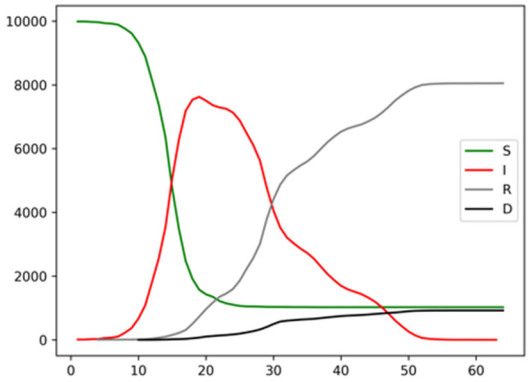

Figure 13. Dynamics of the number of sick, healthy, recovered, and deceased individuals in modeling the Delta strain.

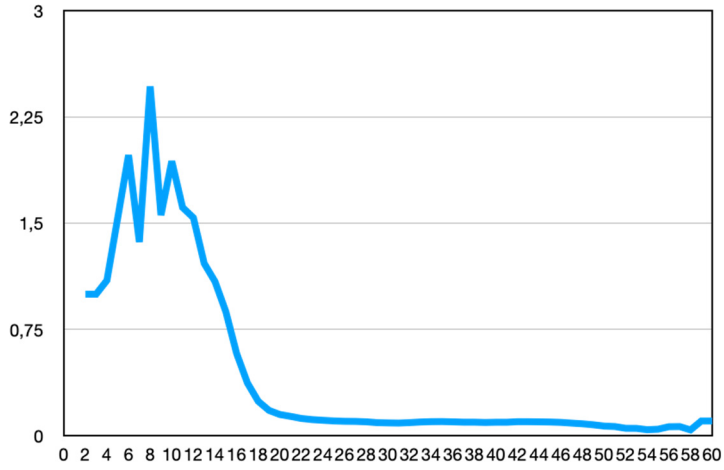

Figure 14. Dynamics of the reproductive number R_0 in modeling the Delta strain.

The graph of the dynamics of infection among immunocompromised individuals clearly shows saturation on the 14th to 15th day (Figure 15). This is also due to the fact that, on the one hand, younger individuals and children, who have a longer incubation period, join the majority of the population, and on the other hand, this population group experiences a significantly longer duration of illness. This means that in the case of such an active virus strain, 80% of these individuals will be infected within the first days of the epidemic. For immunocompetent individuals, this indicator is

Preprints (www.preprints.org) | NOT PEER-REVIEWED | Posted: 12 July 2023 doi:10.20944/preprints202307.0775.v1

70%, and there is no saturation. In other words, after reaching 70%, the epidemic sharply declines. It should be noted that the difference in the reproductive number between these population groups is also significant (Figure 16). Specifically, for immunocompromised individuals, R_0=7.5, while for immunocompetent individuals, R_0=3.1. The difference in the dynamics of infection between these two groups is smaller and amounts to only 2 days, unlike the 5 days for the previous virus strain (Table 6). Therefore, infected immunocompetent individuals start infecting others earlier and become more active sources of transmission compared to the previous case.

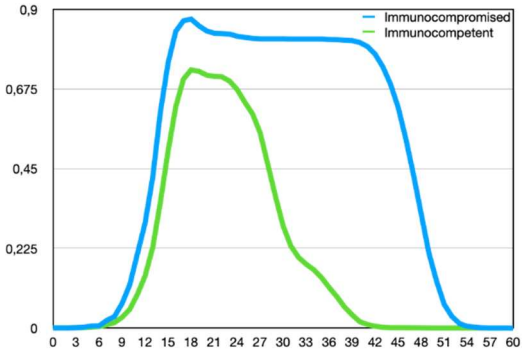

Figure 15. Comparative dynamics of the number of immunocompromised and immunocompetent individuals in modeling the Delta strain.

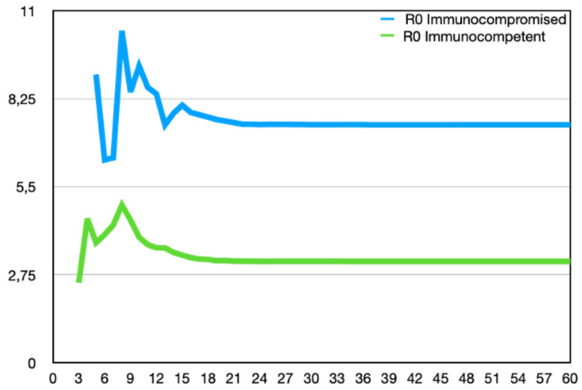

Figure 16. Comparative dynamics of the reproductive number R_0 for immunocompromised and immunocompetent individuals in modeling the Delta strain.

Table 6. The number of days to reach the specified level of infection for the Delta variant depends on immunity.

	Immunocompromised	Immunocompetent	Difference
25%	12	14	2
50%	14	16	2
75%	16	19	3
86%	18		

The main difference in the dynamics of infection among age groups of the population (Figure 17) is the presence of clear saturation for certain groups, such as pregnant women. This means that such an active virus strain is capable of simultaneously infecting 100% of these individuals. Similarly, the group of preschoolers and schoolchildren stands out, as they get infected later and experience significantly fewer cases of illness compared to the general population.

Preprints (www.preprints.org) | NOT PEER-REVIEWED | Posted: 12 July 2023 doi:10.20944/preprints202307.0775.v1

The dynamics of the reproductive number remain similar to the previous virus strain (Figure 18). This means that regardless of the virus strain, the individual infectivity of a respondent no longer plays a significant role. What matters is the circle of contacts and interactions of the infected respondent.

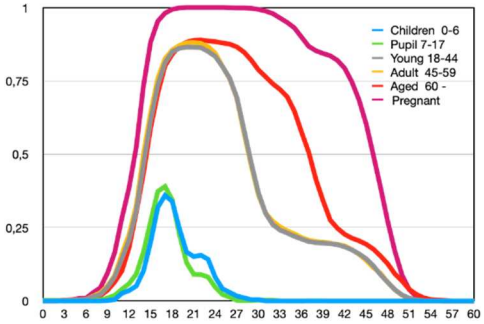

Figure 17. Comparative dynamics of the number of infected individuals across different age groups in modeling the Delta strain.

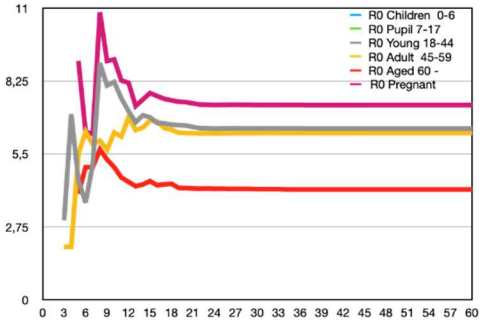

Figure 18. Comparative dynamics of the reproductive number across different age groups in modeling the Delta strain.

The mode of transportation, whether public transport or private car, significantly influences the dynamics of infection (Figure 19). Weekly fluctuations in the graph of people using public transport or walking to work are clearly visible.

The delay in infection is only 1 day (Table 7). However, the reproductive number increases for both cases (Figure 20) (R_0=6.3 for public transport, R_0=4.9 for private cars). The difference between them becomes more significant. This means that people using public transport become more active sources of infection spread than those using private vehicles.

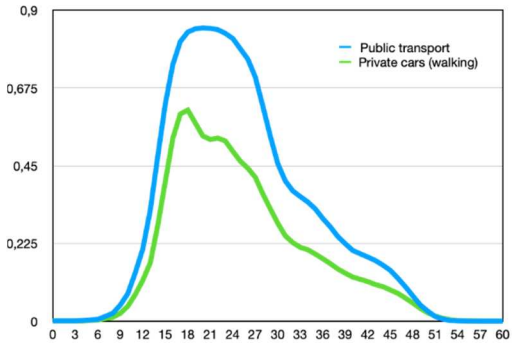

Figure 19. Comparative dynamics of the number of infected individuals based on transportation mode in modeling the Delta strain.

Preprints (www.preprints.org) | NOT PEER-REVIEWED | Posted: 12 July 2023 doi:10.20944/preprints202307.0775.v1

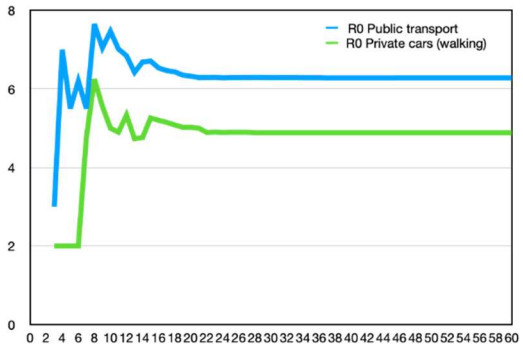

Figure 20. Comparative dynamics of the reproductive number based on transportation mode in modeling the Delta strain.

Table 7. The number of days to reach the specified level of infection for the Delta variant depends on type of transport.

	Public Transport	Private Cars (Walking)	Difference
25%	14	15	1
50%	16	17	1
75%	18		

Similarly, to the previous case, the virus spreads most actively among university faculty and students (Table 8). The next group to be affected is office workers, followed by schools. The lowest number of infections, in the case of a rapid virus strain, occurs among public transport drivers. This can be explained by the virus being highly active, and people spend the majority of their time at their workplaces rather than in transportation.

Table 8. The reproductive number for different professions/specialties for the Delta variant.

Proffesion	R_0
University_Student	6,75
Offices	6,64
Schools	6,47
Grocery	5,97
PreSchools	5,56
Universities	5,17
Retail	3,90
Unemployed	3,77
Domestic	3,57

4.4. Modeling the Spatial Spread of the Omicron Variant

This virus strain is the most aggressive in terms of infectivity among people. It is evident that if no preventive measures are taken, within a short period of 10 days, almost all individuals who come into contact with infected individuals will become infected. The only ones not infected will be those who have not crossed paths with the infected individuals (Figure 21). Thus, on the 10th day, there is a nearly 100% infection rate in the city, leading to a total epidemic. Weekly fluctuations in infections become more pronounced.

The reproductive number reaches its maximum possible level (R_0=8.9) (Figure 22). Over the course of the week, people recover, and the epidemic declines.

Preprints (www.preprints.org) | NOT PEER-REVIEWED | Posted: 12 July 2023 doi:10.20944/preprints202307.0775.v1

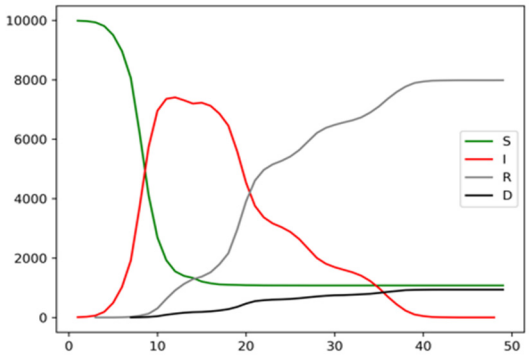

Figure 21. Dynamics of the number of infected, healthy, recovered, and deceased individuals in modeling the Omicron strain.

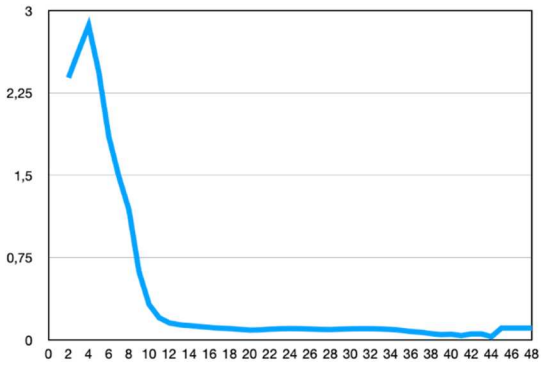

Figure 22. Dynamics of the reproductive number R_0 in modeling the Omicron strain.

The dynamics of all other indicators in most cases are similar to the Delta coronavirus strain, with differences only in absolute values (Figures 22–28, Tables 9 and 10). The following differences should be noted: the difference in infection between immunocompromised and immunocompetent individuals is only 1 day (Table 9). The difference in reproductive numbers for these population groups is at the same level and amounts to 9.3 and 5.1, respectively.

There is also a difference in the reproductive number across age groups (Figure 26). Specifically, the reproductive number for young and middle-aged individuals is approximately the same as for pregnant women. This may be due to the fact that the activity of this virus strain is a more significant factor than the immunity and personal infectivity of an individual. The trends in the corresponding changes of various parameters, depending on the virus strain, confirm the robustness and adequacy of our model.

Table 9. The number of days to reach the specified level of infection for the Omicron strain depends on immunity.

	Immunocompromised	Immunocompetent	Difference
25%	5	6	1
50%	6	7	1
75%	9		

Preprints (www.preprints.org) | NOT PEER-REVIEWED | Posted: 12 July 2023 doi:10.20944/preprints202307.0775.v1

Table 10. The reproductive number for different specialties for the Omicron.

Proffesion	R_0
University_Student	11,42
Universities	10,60
Offices	8,93
PreSchools	7,92
Retail	7,82
Grocery	7,14
Schools	6,76
Unemployed	5,20
Domestic	4,97

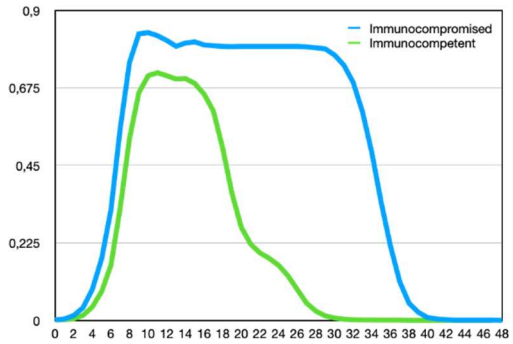

Figure 23. Comparative dynamics of the number of immunocompromised and immunocompetent individuals in modeling the Omicron strain.

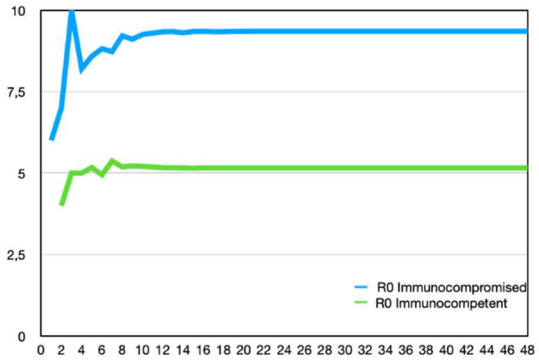

Figure 24. Comparative dynamics of the reproductive number R_0 for immunocompromised and immunocompetent individuals in modeling the Omicron strain.

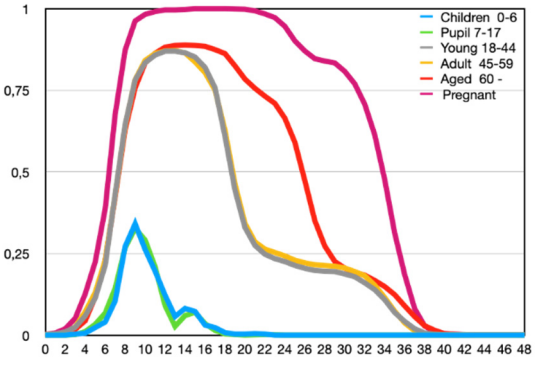

Preprints (www.preprints.org) | NOT PEER-REVIEWED | Posted: 12 July 2023 doi:10.20944/preprints202307.0775.v1

Figure 25. Comparative dynamics of the number of infected individuals across age groups in modeling the Omicron strain.

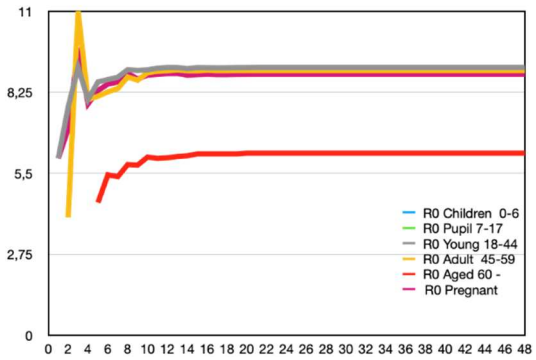

Figure 26. Comparative dynamics of the reproductive number across age groups in modeling the Omicron strain.

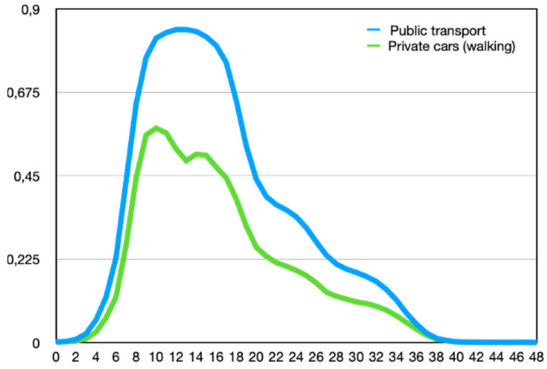

Figure 27. Comparative dynamics of the number of infected individuals depending on the mode of transportation in modeling the Omicron strain.

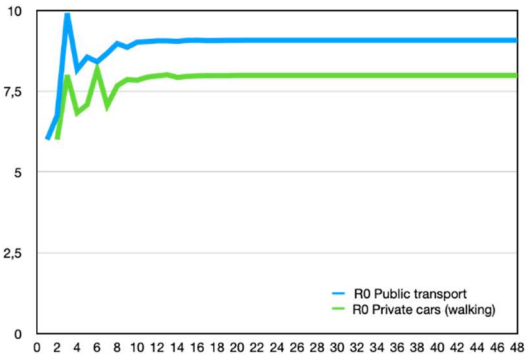

Figure 28. Comparative dynamics of the reproductive number depending on the mode of transportation in modeling the Omicron strain.

5. Conclusions

In the study, a modification of the previously developed GeoSER(D) model was proposed by refining the age structure of the population, incorporating individual schedules for weekdays and workdays, and considering individual health characteristics of agents. This allowed for the construction of a more realistic model of city functioning. The developed model enabled the simulation of the spread of three strains of the COVID-19 virus and the analysis of the model's adequacy in the case of unimpeded virus transmission among city residents.

The following results were obtained:

1. SARS-CoV-2 primarily spreads through contact in workplaces and public transportation, while school children and preschoolers are the consequence rather than the initiators of the epidemic.
2. Fluctuations in the dynamics of different indicators of SARS-CoV-2 transmission are associated with variations in daily schedules between weekdays and weekends. It was shown that the daily schedule of individuals significantly influences the spread of SARS-CoV-2.
3. For more contagious "fast" strains of SARS-CoV-2 (e.g., Omicron), immunocompetent individuals become significant sources of infection. For less contagious "slow" strains (e.g., Alpha) of SARS-CoV-2, immunocompromised individuals (such as pregnant women) are the most active sources of infection.
4. More contagious "fast" strains of the SARS-CoV-2 virus (e.g., Omicron) spread more rapidly in public transportation. For less contagious "slow" strains (e.g., Alpha) of the virus, the highest infection rates occur through work and educational contacts.

Therefore, all of these findings underscore the adequacy and accuracy of the model. This implies that the developed model can be further utilized for analyzing and constructing optimal strategies to prevent epidemic spread. It can also be expanded to encompass regions within a country and even worldwide.

6. Patents

Funding: The study was created within the framework of the project financed by the National Research Fund of Ukraine, registered No. 30/0103 from 01.05.2023, "Methods and means of researching markers of ageing and their influence on post-ageing effects for prolonging the working period", which is carried out at the Department of Artificial Intelligence Systems of the Institute of Computer Sciences and Information of technologies of the National University "Lviv Polytechnic".

References

1. World health statistics 2022: monitoring health for the SDGs, sustainable development goals ISBN 978-92-4-005114-0 (electronic version), ISBN 978-92-4-005115-7 (print version)
2. Jones KE, Patel NG, Levy MA, Storeygard A, Balk D, Gittleman JL, et al. “Global trends in emerging infectious diseases”. Nature. 2008;451(7181):990–3.
3. Wilder-Smith A, Gubler DJ. “Geographic expansion of dengue: the impact of international travel.” Med Clin North Am. 2008;92(6):1377–90.
4. Wilder-Smith, A. “COVID-19 in comparison with other emerging viral diseases: risk of geographic spread via travel”. Trop Dis Travel Med Vaccines 7, 3 (2021). https://doi.org/10.1186/s40794-020-00129-9
5. Wang L, Alexander CA. “COVID-19 Compared with Other Viral Diseases: Novelties, Progress, and Challenges”. Electron J Gen Med. 2021;18(1):em265. https://doi.org/10.29333/ejgm/8575
6. Myron S. Cohen And Lawrence Corey “Combination prevention for COVID-19”. Science, 8 May 2020, Vol 368, Issue 6491, p. 551, DOI: 10.1126/science.abc579
7. Kumala, R. D. M. (2020). Legal Analysis of Government Policy on Large Scale Social Restrictions in Handling Covid-19. The Indonesian Journal of International Clinical Legal Education, 2(2), 181-200. https://doi.org/10.15294/ijicle.v2i2.38326
8. Jeanne-Marie Hament, Jan L.L. Kimpen, Andre Fleer, Tom F.W. Wolfs, “Respiratory viral infection predisposing for bacterial disease: a concise review”, FEMS Immunology & Medical Microbiology, Volume 26, Issue 3-4, December 1999, Pages 189–195, https://doi.org/10.1111/j.1574-695X.1999.tb01389.x
9. Gould, D., Patel, A., Becker, G. et al. “SIR/RSNA/CIRSE Joint Medical Simulation Task Force Strategic Plan: Executive Summary”. Cardiovasc Intervent Radiol 30, 551–554 (2007). https://doi.org/10.1007/s00270-007-9103-9
10. Chatterjee, Amar Nath, Fahad Al Basir, Dibyendu Biswas, and Teklebirhan Abraha. "Global Dynamics of SARS-CoV-2 Infection with Antibody Response and the Impact of Impulsive Drug Therapy." Vaccines 10, no. 11 (2022): 1846.
11. Chatterjee, Amar Nath, and Bashir Ahmad. "A fractional-order differential equation model of COVID-19 infection of epithelial cells." Chaos, Solitons & Fractals 147 (2021): 110952.
12. Li M Y, Graef JR, Wang L, Karsai J. 1999 “Global dynamics of a SEIR model with varying total population size”. Mathematical biosciences 160, 191–213.

13. Freihat, Asad A. and Handam, Ali H. "Solution of the SIR models of epidemics using MSGDTM", Applications and Applied Mathematics: An International Journal (AAM), Vol. 9, Iss. 2, Article 11. 2014. Available at: https://digitalcommons.pvamu.edu/aam/vol9/iss2/11
14. Constantinos I. Siettos & Lucia Russo (2013) Mathematical modeling of infectious disease dynamics, Virulence, 4:4, 295-306, DOI: 10.4161/viru.24041
15. Liberati, A., Altman, D. G., Tetzlaff, J., Mulrow, C., Gøtzsche, P. C., Ioannidis, J. P., ... & Moher, D. (2009). The PRISMA statement for reporting systematic reviews and meta-analyses of studies that evaluate health care interventions: explanation and elaboration. Annals of internal medicine, 151(4), W-65. https://doi.org/10.7326/0003-4819-151-4-200908180-00136
16. Y. Xiao, M. Yang, Z. Zhu, H. Yang, L. Zhang, and S. Ghader, "Modeling indoor-level non-pharmaceutical interventions during the COVID-19 pandemic: a pedestrian dynamics-based microscopic simulation approach," Transport Policy, 2021.
17. J. J. Fruin, Designing for Pedestrians: A Level of Service Concept vol. 355: Polytechnic University, 1970.
18. K. Teknomo, Y. Takeyama, and H. Inamura, "Review on microscopic pedestrian simulation model," arXiv preprint arXiv:1609.01808, 2016.
19. G. N. Sze-To, Y. Yang, J. K. Kwan, S. C. Yu, and C. Y. Chao, "Effects of surface material, ventilation, and human behavior on indirect contact transmission risk of respiratory infection," Risk analysis, vol. 34, pp. 818-830, 2014.
20. S. Namilae, A. Srinivasan, A. Mubayi, M. Scotch, and R. Pahle, "Self-propelled pedestrian dynamics model: Application to passenger movement and infection propagation in airplanes," Physica A: Statistical Mechanics and its Applications, vol. 465, pp. 248-260, 2017.
21. D. A. Goldmann, "Transmission of viral respiratory infections in the home," The Pediatric infectious disease journal, vol. 19, pp. S97-S102, 2000.
22. P. H. Schimit, "A model based on cellular automata to estimate the social isolation impact on COVID-19 spreading in Brazil," Computer Methods and Programs in Biomedicine, vol. 200, p. 105832, 2021.
23. P. Patlolla, V. Gunupudi, A. R. Mikler, and R. T. Jacob, "Agent-based simulation tools in computational epidemiology," in International Workshop on Innovative Internet Community Systems, 2004, pp. 212-223.
24. S. Bin, G. Sun, and C.-C. Chen, "Spread of infectious disease modeling and analysis of different factors on spread of infectious disease based on cellular automata," International Journal of Environmental Research and Public Health, vol. 16, p. 4683, 2019.
25. A. L. B. Cavalcante, L. P. de Faria Borges, M. A. da Costa Lemos, M. M. de Farias, and H. S. Carvalho, "Modelling the spread of covid-19 in the capital of Brazil using numerical solution and cellular automata," Computational Biology and Chemistry, vol. 94, p. 107554, 2021.
26. I. Lugo and M. G. Alatriste-Contreras, "Intervention strategies with 2D cellular automata for testing SARS-CoV-2 and reopening the economy," Research Square, 2020.
27. Y. Vyklyuk, M. Manylich, M. Škoda, M. M. Radovanović, and M. D. Petrović, "Modeling and analysis of different scenarios for the spread of COVID-19 by using the modified multi-agent systems–Evidence from the selected countries," Results in Physics, vol. 20, p. 103662, 2021.
28. T. Xiao, T. Mu, S. Shen, Y. Song, S. Yang, and J. He, "A dynamic physical-distancing model to evaluate spatial measures for prevention of Covid-19 spread," Physica A: Statistical Mechanics and its Applications, vol. 592, p. 126734, 2022.
29. S. Mukherjee, S. Mondal, and B. Bagchi, "Dynamical theory and cellular automata simulations of pandemic spread: Understanding different temporal patterns of infections," arXiv:2004.14787, 2020.
30. E. Hosseini, K. Z. Ghafoor, A. S. Sadiq, M. Guizani, and A. Emrouznejad, "Covid-19 optimizer algorithm, modeling and controlling of coronavirus distribution process," IEEE Journal of Biomedical and Health Informatics, vol. 24, pp. 2765-2775, 2020.
31. Y. Kim, H. Ryu, and S. Lee, "Agent-based modeling for super-spreading events: A case study of MERS-CoV transmission dynamics in the Republic of Korea," International Journal of Environmental Research and Public Health, vol. 15, p. 2369, 2018.
32. J. B. Dunham, "An agent-based spatially explicit epidemiological model in MASON," Journal of Artificial Societies and Social Simulation, vol. 9, 2005.
33. M. Shamil, F. Farheen, N. Ibtehaz, I. M. Khan, and M. S. Rahman, "An agent-based modeling of COVID-19: validation, analysis, and recommendations," Cognitive Computation, pp. 1-12, 2021.
34. A. A. Alzu'bi, S. I. A. Alasal, and V. J. Watzlaf, "A simulation study of coronavirus as an epidemic disease using agent-based modeling," Perspectives in Health Information Management, vol. 18, 2021.
35. Varun Kompella, Roberto Capobianco, Stacy Jong, Jonathan Browne, Spencer Fox, Lauren Meyers, Peter Wurman, Peter Stone "Reinforcement Learning for Optimization of COVID-19 Mitigation policies", arXiv:2010.10560, https://doi.org/10.48550/arXiv.2010.10560
36. Fujita, S., Kiguchi, R., Yoshida, Y. et al. "Determination of optimal prevention strategy for COVID-19 based on multi-agent simulation". Jpn J Stat Data Sci 5, 339–361, 2022. https://doi.org/10.1007/s42081-022-00163-1

37. Imran Mahmood, Hamid Arabnejad, Diana Suleimenova, Isabel Sassoon, Alaa Marshan, Alan Serrano-Rico, Panos Louvieris, Anastasia Anagnostou, Simon J E Taylor, David Bell & Derek Groen "FACS: A geospatial agent-based simulator for analysing COVID-19 spread and public health measures on local regions", Journal of Simulation, 16:4, 355-373, (2022) DOI:10.1080/17477778.2020.1800422
38. G. Ortigoza, F. Brauer, and I. Neri, "Modelling and simulating Chikungunya spread with an unstructured triangular cellular automata," Infectious Disease Modelling, vol. 5, pp. 197-220, 2020.
39. L. Perez and S. Dragicevic, "An agent-based approach for modeling dynamics of contagious disease spread," International Journal of Health Geographics, vol. 8, pp. 1-17, 2009.
40. J. Munshi, I. Roy, and G. Balasubramanian, "Spatiotemporal dynamics in demography-sensitive disease transmission: COVID-19 spread in NY as a case study," arXiv:2005.01001, 2020.
41. M. Ajelli, B. Gonçalves, D. Balcan, V. Colizza, H. Hu, J. J. Ramasco, et al., "Comparing large-scale computational approaches to epidemic modeling: agent-based versus structured metapopulation models," BMC Infectious Diseases, vol. 10, pp. 1-13, 2010.
42. Yaroslav Vyklyuk, Denys Nevinskyi, Nataliya Boyko. GeoCity: A New Dynamic-SPATIAL Model of Urban Ecosystem J. Geogr. Inst. Cvijic. 2023, (in press)
43. State Statistics Service Of Ukraine. https://www.ukrstat.gov.ua